

# SUSY Signals at HERA in the No-Scale Flipped $SU(5)$ Supergravity Model

JORGE L. LOPEZ<sup>(a)(b)</sup>, D. V. NANOPOULOS<sup>(a)(b)</sup>, XU WANG<sup>(a)(b)</sup>, and A. ZICHICHI<sup>(c)</sup>

<sup>(a)</sup> *Center for Theoretical Physics, Department of Physics, Texas A&M University  
College Station, TX 77843-4242, USA*

<sup>(b)</sup> *Astroparticle Physics Group, Houston Advanced Research Center (HARC)  
The Woodlands, TX 77381, USA*

<sup>(c)</sup> *CERN, Geneva, Switzerland*

## ABSTRACT

Sparticle production and detection at HERA are studied within the recently proposed no-scale flipped  $SU(5)$  supergravity model. Among the various reaction channels that could lead to sparticle production at HERA, only the following are within its limit of sensitivity in this model:  $e^-p \rightarrow \tilde{e}_{L,R}^- \chi_i^0 + X, \tilde{\nu}_e \chi_1^- + X$ , where  $\chi_i^0 (i = 1, 2)$  are the two lightest neutralinos and  $\chi_1^-$  is the lightest chargino. We study the elastic and deep-inelastic contributions to the cross sections using the Weizsäcker-Williams approximation. We find that the most promising supersymmetric production channel is right-handed selectron ( $\tilde{e}_R$ ) plus first neutralino ( $\chi_1^0$ ), with one hard electron and missing energy signature. The  $\tilde{\nu}_e \chi_1^-$  channel leads to comparable rates but also allows jet final states. A right-handedly polarized electron beam at HERA would shut off the latter channel and allow preferentially the former one. With an integrated luminosity of  $\mathcal{L} = 100 \text{ pb}^{-1}$ , HERA can extend the present LEPI lower bounds on  $m_{\tilde{e}_R}, m_{\tilde{\nu}_e}, m_{\chi_1^0}$  by  $\approx 25 \text{ GeV}$ , while  $\mathcal{L} = 1000 \text{ pb}^{-1}$  will make HERA competitive with LEP II. We also show that the Leading Proton Spectrometer (LPS) at HERA is an excellent supersymmetry detector which can provide indirect information about the sparticle masses by measuring the leading proton longitudinal momentum distribution.

April, 1993

## 1. Introduction

The search for supersymmetric (SUSY) particles using existing facilities is the crucial problem for particle physicists nowadays. One of the most important reasons to study detailed spectra and properties of the expected SUSY particles on the basis of well motivated theoretical concepts, is that quite a few particle accelerators are either running (Tevatron, LEP1, SLC, HERA) or will become operational in the near future (LEP2) and their center-of-mass energy is within the range of the sparticle masses. Using two well motivated supersymmetric (the minimal  $SU(5)$  [1] and the no-scale flipped  $SU(5)$  [2] supergravity) models, we have previously discussed the possible SUSY production channels and detection signatures at the Tevatron [3] and at LEP2 [4]. In this paper we continue this program applying it to the HERA  $e^-p$  collider within the context of the same two models. Fortunately or unfortunately, the minimal  $SU(5)$  supergravity model is out of the reach of HERA because the slepton and squark masses ( $\gtrsim 500$  GeV) are too large to be kinematically accessible. On the other hand, in the no-scale flipped  $SU(5)$  supergravity model, the slepton and squark masses are much lighter and part of the parameter space can be explored at HERA. However, since the squark masses are always above 200 GeV, the much studied production channels involving squarks [5] are highly suppressed and are neglected in this paper. Therefore, we focus on the production of sleptons, charginos, and neutralinos at HERA within the predictions of the no-scale flipped  $SU(5)$  supergravity model. It is interesting to remark that in contrast with “generic” supersymmetric models where the squarks can arbitrarily be taken to be light or heavy, this is not an option in this model, that is, HERA should *not* produce squarks if this model is correct.

The production processes of interest at HERA are

$$e^-p \rightarrow \tilde{e}_{L,R}^- \chi_{1,2}^0 + X, \quad (1.1a)$$

$$e^-p \rightarrow \tilde{\nu}_e \chi_1^- + X, \quad (1.1b)$$

both of which have very small Standard Model backgrounds. Indeed,  $\sigma(ep \rightarrow \nu_e W + p, W \rightarrow e\bar{\nu}_e) \approx 10^{-3}$  pb and  $\sigma(ep \rightarrow eZ + p, Z \rightarrow \nu\bar{\nu}) \approx 7 \times 10^{-3}$  pb [6]. Moreover, by measuring the total  $\nu_e W$  and  $eZ$  cross sections through the other decay modes of the  $W$  and  $Z$  one could in principle subtract off these backgrounds [7]. The processes in Eq. (1.1) receive elastic ( $Q^2 < 4$  GeV), deep-inelastic ( $Q^2 > 4$  GeV), and inelastic contributions, where  $-Q^2$  is the exchanged virtual photon mass squared. It has been shown [8] that the cross section for the inelastic processes, whereby the proton gets excited into various

resonances, is smaller than that for the other two. We neglect its contribution in our calculations. This makes our results conservative as far as the sparticle mass lower bound that can be explored at HERA is concerned. Also, the exact calculation of the total cross section for the processes mentioned above usually involves the numerical evaluation of a three- (or more) body phase space which is rather time-consuming because of the large size of the parameter space to be scanned. For this reason we use the Weizsäcker-Williams (WW) [9] approximation scheme proposed in Refs. [6,7]. In this method the  $e\gamma$  reaction is treated as a subprocess with a real (on-shell) photon. By incorporating the density distribution of photons inside protons or quarks, one can get reasonable approximations to the total cross sections.

The signature for selectron-neutralino production is dominated by  $\tilde{e}_R\chi_1^0$  and consists of one outgoing hard electron plus missing transverse momentum ( $\cancel{p}_T$ ). There is a small contribution from  $\tilde{e}_R\chi_2^0$  production which can produce trilepton ( $\chi_2^0 \rightarrow l^+l^- + \chi_1^0$ ) or mixed ( $\chi_2^0 \rightarrow 2\text{jets} + \chi_1^0$ ) signals. Chargino-sneutrino production can also lead to one outgoing hard lepton since the chargino can decay leptonically and the sneutrino decays mostly invisibly ( $\tilde{\nu}_e \rightarrow \nu_e + \chi_1^0$ )

This paper is organized as follows. First we discuss the features of the no-scale flipped  $SU(5)$  supergravity model (Sec. 2). Then we give the exact formulae for the relevant tree-level cross sections in the WW approximation (Sec. 3), followed by the results of the calculation (Sec. 4). Finally we discuss the phenomenological implications of our work (Sec. 5).

## 2. The no-scale flipped $SU(5)$ supergravity model [2]

This supersymmetric model can be viewed as a specific subset of the minimal supersymmetric standard model (MSSM), in that its three-dimensional parameter space is contained in the 21-dimensional parameter space of the MSSM. This subset is not arbitrary, but determined by the application of several well motivated theoretical constraints. In this model it is assumed that below the Planck scale the gauge group is flipped  $SU(5)$ , with some special properties expected from a superstring-derived model, that is, it is a string-inspired model. For example, gauge coupling unification occurs at the scale  $M_U = 10^{18}$  GeV, in contrast with  $10^{16}$  GeV for the minimal  $SU(5)$  model. Moreover, the usual supergravity-induced universal soft-supersymmetry breaking parameters are assumed to obey  $m_0 = A = 0$ , as is the case in typical no-scale supergravity models [10].

Thus the only three parameters in this model are: the top-quark mass ( $m_t$ ), the ratio of Higgs vacuum expectation values ( $\tan\beta$ ), and the gluino mass ( $m_{\tilde{g}}$ ). Through the running of the renormalization group equations and the minimization of the one-loop effective potential, one can obtain the whole set of masses and couplings (including the one-loop corrected Higgs boson masses) in this model for each allowed point in parameter space [11]. In what follows we take  $m_t = 100, 130, 160$  GeV, for which we find  $2 < \tan\beta < 32$ .

Clearly, the several sparticle masses will be correlated, and are found to scale with the gluino mass. Of great relevance is the fact that the present body of phenomenological constraints on the sparticle masses disallows certain combinations of the parameters, in particular one obtains

$$m_{\tilde{g}} \approx m_{\tilde{q}} \gtrsim 200 \text{ GeV}. \quad (2.1)$$

Also, most of the weakly interacting sparticles cannot be too heavy. In fact, we take the “no-scale inspired” condition  $m_{\tilde{g},\tilde{q}} \lesssim 1 \text{ TeV}$  to hold. One finds

$$\begin{aligned} m_{\tilde{e}_R} < 190 \text{ GeV}, \quad m_{\tilde{e}_L} < 305 \text{ GeV}, \quad m_{\tilde{\nu}} < 295 \text{ GeV}, \quad m_{\tilde{\tau}_1} < 185 \text{ GeV}, \quad m_{\tilde{\tau}_2} < 315 \text{ GeV}, \\ m_h < 135 \text{ GeV}, \quad m_{\chi_1^0} < 145 \text{ GeV}, \quad m_{\chi_2^0} < 285 \text{ GeV}, \quad m_{\chi_1^\pm} < 285 \text{ GeV}. \end{aligned} \quad (2.2)$$

There are also simple approximate relations that these masses obey, namely

$$m_{\tilde{e}_L} \sim 0.3 m_{\tilde{g}}; \quad m_{\tilde{e}_R} \sim 0.18 m_{\tilde{g}}, \quad (2.3a)$$

$$m_{\chi_1^0} \sim \frac{1}{2} m_{\chi_2^0}; \quad m_{\chi_2^0} \approx m_{\chi_1^\pm} \sim 0.3 m_{\tilde{g}}. \quad (2.3b)$$

For low  $m_{\tilde{g}}$ , the sneutrino mass is close to  $m_{\tilde{e}_R}$ ; as  $m_{\tilde{g}}$  grows, the sneutrino mass approaches  $m_{\tilde{e}_L}$ . Note that  $m_{\tilde{e}_R}/m_{\tilde{e}_L} \approx 0.6$ , in sharp contrast with usual approximation of degenerate selectron masses. For more details on the construction of this model we refer the reader to Ref. [2].

### 3. The allowed production processes

The relevant Feynman diagrams for the sparticle production channels in Eq. (1.1) are shown in Fig. 1 for the elastic contributions. The deep-inelastic processes receive contributions analogous to those shown in Fig. 1 with the replacement *proton* for *parton*, plus additional production diagrams involving squark exchanges. Since it has been shown [8] that the squark contributions to the cross sections for this type of deep-inelastic processes are negligible for  $m_{\tilde{q}} \gtrsim 200 \text{ GeV}$ , which is the case in this model (see Sec. 2), in what

follows we neglect all diagrams involving squarks. We also remark that in this model the masses of the right- and left-handed selectrons are highly non-degenerate (see Sec. 2), in sharp contrast with the approximation of degenerate selectron masses usually made in the literature. The squared amplitude for the subprocess  $e\gamma \rightarrow \tilde{e}_{L,R}\chi_1^0$  (for unpolarized incident electrons) is given by

$$|\mathcal{M}_{L,R}|^2 = \frac{1}{2}e^6 f_{L,R}^2 \frac{1}{Q^4} \left\{ \frac{4}{\hat{s}^2} (m_{\chi_i^0}^2 - m_{\tilde{e}_{L,R}}^2) p_1^\mu p_1^\nu + \left[ 4 \frac{(m_{\chi_i^0}^2 - m_{\tilde{e}_{L,R}}^2)}{(\hat{u} - m_{\tilde{e}_{L,R}}^2)^2} - \frac{4q^2}{\hat{s}(\hat{u} - m_{\tilde{e}_{L,R}}^2)} \right] p_2^\mu p_2^\nu \right. \\ \left. + \left[ \frac{q^2}{\hat{s}^2} (m_{\chi_i^0}^2 - m_{\tilde{e}_{L,R}}^2) + \frac{1}{\hat{s}} (\hat{t} - m_{\chi_i^0}^2) \right] g^{\mu\nu} \right. \\ \left. + \frac{2[2(m_{\chi_i^0}^2 - m_{\tilde{e}_{L,R}}^2) + q^2]}{\hat{s}(\hat{u} - m_{\tilde{e}_{L,R}}^2)} (p_1^\mu p_2^\nu + p_1^\nu p_2^\mu) \right\} \cdot \frac{1}{2}(-g_{\mu\nu}), \quad (3.1)$$

where  $p_1$  ( $p_2$ ) is the electron (selectron) momentum, and  $\hat{s}, \hat{t} = (p_1 - p_2)^2$ ,  $\hat{u}$  are the Mandelstam variables for this subprocess. The coupling factors  $f_{L,R}$  are

$$f_L = \frac{\sqrt{2}}{e} \left[ eN'_{i1} + \frac{g}{\cos\theta_W} \left( \frac{1}{2} - \sin^2\theta_W \right) N'_{i2} \right], \quad (3.2a)$$

$$f_R = -\frac{\sqrt{2}}{e} \left[ eN'_{i1} - \frac{g \sin^2\theta_W}{\cos\theta_W} N'_{i2} \right], \quad (3.2b)$$

with

$$N'_{i1} = N_{i1} \cos\theta_W + N_{i2} \sin\theta_W, \quad N'_{i2} = -N_{i1} \sin\theta_W + N_{i2} \cos\theta_W, \quad (3.3)$$

where  $N_{i1}, N_{i2}$  are elements of the matrix diagonalizing the neutralino mass matrix. Here we follow the conventions of Ref. [12]. The squared amplitude of the subprocess  $e\gamma \rightarrow \tilde{\nu}_e\chi_1^-$  is given by

$$|\mathcal{M}|^2 = \frac{1}{2}e^4 f_L'^2 \frac{1}{Q^4} \left\{ \left[ \frac{4}{\hat{s}^2} (m_{\chi_1^-}^2 - m_{\tilde{\nu}_e}^2) + \frac{4q^2}{\hat{s}(\hat{u} - m_{\chi_1^-}^2)} \right] p_1^\mu p_1^\nu + \left[ \frac{4(m_{\chi_1^-}^2 - m_{\tilde{\nu}_e}^2)}{(\hat{u} - m_{\chi_1^-}^2)^2} + \frac{4q^2}{\hat{s}(\hat{u} - m_{\chi_1^-}^2)} \right] p_2^\mu p_2^\nu \right. \\ \left. + \left[ \hat{s}(\hat{u} - m_{\chi_1^-}^2) + q^2(m_{\chi_1^-}^2 - m_{\tilde{\nu}_e}^2) \right] \left[ \frac{1}{\hat{s}} + \frac{1}{\hat{u} - m_{\chi_1^-}^2} \right]^2 g^{\mu\nu} \right. \\ \left. + \frac{4(m_{\chi_1^-}^2 - m_{\tilde{\nu}_e}^2 - q^2)}{\hat{s}(\hat{u} - m_{\chi_1^-}^2)} (p_1^\mu p_2^\nu + p_1^\nu p_2^\mu) \right\} \cdot \frac{1}{2}(-g_{\mu\nu}), \quad (3.4)$$

where  $p_1$  ( $p_2$ ) is the electron (chargino) momentum, and  $f_L' = gV_{11}$ , with  $V_{11}$  is an element of the matrix diagonalizing the chargino mass matrix [12].

The Weisäcker-Williams (WW) approximation [9] is now used to simplify the calculation. For elastic processes we use the following photon distribution in the proton [7]

$$f_{\gamma|p}(z) = \frac{\alpha}{2\pi z} [1 + (1-z)^2] \left[ \ln A - \frac{11}{6} + \frac{3}{A} - \frac{3}{2A^2} + \frac{1}{3A^2} \right], \quad (3.5)$$

where  $A = 1 + (0.71 \text{ GeV}^2)/Q_{min}^2$  and

$$Q_{min}^2 = -2m_p^2 + \frac{1}{2s} \left[ (s + m_p^2)(s - \hat{s} + m_p^2) - (s - m_p^2) \sqrt{(s - \hat{s} - m_p^2)^2 - 4m_p^2 \hat{s}} \right]. \quad (3.6)$$

The total elastic cross section for  $ep \rightarrow Xp$  can then be written as

$$\sigma_{elastic}(ep \rightarrow Xp) = \int_{z_{min}}^{z_{max}} dz f_{\gamma|p}(z) \hat{\sigma}(\hat{s}), \quad (3.7)$$

where  $\hat{\sigma}(\hat{s})$  is the total subprocess cross section for the real  $\gamma e \rightarrow X$  process (*i.e.*, Eqs. (3.1), (3.4) integrated over the  $X$ -phase space), and  $z = \hat{s}/s$ , where  $\hat{s}$  is the center-of-mass energy of the subprocess. For a two-body final state  $X$  with particles of masses  $\tilde{m}_1$  and  $\tilde{m}_2$ , one has

$$z_{min} = \frac{1}{s} (\tilde{m}_1 + \tilde{m}_2)^2. \quad (3.8)$$

Also,  $z_{max} = (1 - m_p/\sqrt{s})^2$ . For the deep-inelastic processes we use the photon distribution in the quark of Ref. [6],

$$P_{\gamma|q_f}(\eta) = \frac{\alpha}{2\pi} e_{q_f}^2 \frac{1 + (1-\eta)^2}{\eta} \ln \frac{t_{max}}{t_{cut}}, \quad (3.9)$$

where  $t_{max} = xs - (\tilde{m}_1 + \tilde{m}_2)^2$  and  $t_{cut} = 4 \text{ GeV}^2$  are the limits put on  $Q^2$  for the deep-inelastic process. Also,  $e_{q_f}$  is the electric charge of the  $q_f$  quark,  $x$  is the parton density distribution variable, and  $\eta = z/x$ . The total cross section for the deep-inelastic processes is thus given by [6]

$$\sigma_{deep-inelastic}(e \text{ parton} \rightarrow X \text{ parton}) = \int_{z_{min}}^1 dx \sum_f q_f(x, Q^2) \int_{\frac{1}{x} z_{min}}^1 d\eta P_{\gamma|q_f}(\eta) \hat{\sigma}(\hat{s}), \quad (3.10)$$

where the parton distribution functions of Ref. [13] have been used, with the energy scale  $Q^2 = (t_{max} - t_{cut})/\ln(t_{max}/t_{cut})$ .

It has been observed that by using the WW approximation, the results are usually larger than the exact results by 20 – 30% for the elastic case [7]. However, for the deep-inelastic processes the WW results are smaller than the exact ones [6]. Consequently the WW approximation will not enhance the effects and is thus good enough in light of the inherent uncertainties in this type of calculations. Moreover, these shifts in the cross sections are equivalent to shifts in the selectron or chargino masses of 5 GeV or less.

## 4. Results

### 4.1. Selectron-neutralino production

There are four possible production channels at HERA

$$ep \rightarrow \tilde{e}_R \chi_1^0, \tilde{e}_R \chi_2^0, \tilde{e}_L \chi_1^0, \tilde{e}_L \chi_2^0 + X. \quad (4.1)$$

By far the largest cross section is for the  $\tilde{e}_R \chi_1^0$  channel. The main reason for this is that in this model the  $\tilde{e}_R$  mass is much smaller than the  $\tilde{e}_L$  mass (see Eq. (2.3a)), and the first neutralino  $\chi_1^0$  is the lightest SUSY particle (LSP), which escapes detection. By the same kinematical reasons the  $\tilde{e}_R \chi_2^0$  and  $\tilde{e}_L \chi_1^0$  cross sections are smaller but still observable, whereas the  $\tilde{e}_L \chi_2^0$  contribution is negligible ( $< 10^{-3}$  pb). This pattern holds for both elastic and deep-inelastic processes. The above sparticles decay mostly in the following ways

$$\tilde{e}_L \rightarrow e_L \chi_1^0, \quad (4.2a)$$

$$\tilde{e}_R \rightarrow e_R \chi_1^0, \quad (4.2b)$$

$$\chi_2^0 \rightarrow \nu_l \bar{\nu}_l \chi_1^0, l^+ l^- \tilde{\chi}_1^0, q \bar{q} \chi_1^0. \quad (4.2c)$$

However, in this model there are some points in the parameter space that also allow the rare decay channels  $\tilde{e}_L \rightarrow e_L \chi_2^0$  and  $\tilde{e}_R \rightarrow e_R \chi_2^0$ . These only contribute for a small region of parameter space ( $\approx 12\%$  of the allowed points) and are phase space suppressed. The cross section for the dominant elastic  $ep \rightarrow \tilde{e}_R \chi_1^0 \rightarrow ep + \not{p}$  and deep-inelastic  $ep \rightarrow \tilde{e}_R \chi_1^0 \rightarrow eX + \not{p}$  processes are shown in the top row of Fig. 2 and 3 respectively. Note that for increasingly larger selectron masses, the cross section for the deep-inelastic process drops faster than that for the elastic one. The analogous results for the smaller  $\tilde{e}_R \chi_2^0$  and  $\tilde{e}_L \chi_1^0$  channels are shown in the bottom row of Figs. 2,3.

Let us consider the four elastic cross sections  $\sigma(\tilde{e}_{R,L} \chi_{1,2}^0)$  in order to disentangle the best signal to be experimentally detected. According to Ref. [7], the cross section for the elastic processes (Eq. (4.1)) peaks at a value ( $p_e^*$ ) of the daughter electron transverse momentum given by

$$p_e^* = \frac{m_{\tilde{e}_{R,L}}^2 - m_{\chi_{1,2}^0}^2}{2m_{\tilde{e}_{R,L}}}. \quad (4.3)$$

Moreover, a Monte-Carlo study shows that the average transverse momentum is close to  $\langle p_T^e \rangle \approx p_e^*$ . To get an idea of the most likely values of  $p_T^e$ , we have computed the average  $\tilde{p}_e^*$  (weighed by the four elastic cross sections) and the results are shown in Fig. 4. Clearly,

the daughter electrons will be hard and with large  $p_T$ . This is an excellent signal to be detected at HERA.

For elastic processes, another measurable signal is the slowed down outgoing proton. Since the transverse momentum of the outgoing proton is very small, the relative energy loss of the proton energy  $z = (E_p^{in} - E_p^{out})/E_p^{in}$  is given by  $z = 1 - x_L$ , where  $x_L$  is the longitudinal momentum of the leading proton. It has been pointed out [7] that the  $z$ -distribution is peaked at a value not much larger than its minimal value,

$$z_{min} = \frac{1}{s}(m_{\tilde{e}_{R,L}} + m_{\chi_{1,2}^0})^2. \quad (4.4)$$

Therefore, the smallest measured value in the  $z$ -distribution should be a good approximation to  $z_{min}$ . Since the Leading Proton Spectrometer (LPS) of the ZEUS detector at HERA can measure this distribution accurately, one may have a new way of probing the supersymmetric spectrum, as follows. We calculate the average  $\tilde{z}_{min}$  weighed by the different elastic cross sections  $\sigma(\tilde{e}_{R,L}\chi_{1,2}^0)$ . The results are shown in the top row of Fig. 5 versus the total elastic cross section. These plots show the possible values of  $\tilde{z}_{min}$  for a given sensitivity. For example, if elastic cross sections could be measured down to  $\approx 10^{-3}$  pb, then  $\tilde{z}_{min}$  could be probed up to  $\approx 0.2$ . Now,  $\tilde{z}_{min}$  can be computed from Eq. (4.4) and be plotted against, say  $m_{\tilde{e}_R}$ , as shown in the bottom row of Fig. 5. For the example given above ( $\tilde{z}_{min} \lesssim 0.2$ ) one could indirectly probe  $\tilde{e}_R$  masses as high as  $\approx 115$  GeV. Note that a useful constraint on  $m_{\tilde{e}_R}$  is possible because the correlation among the various sparticle masses in this model makes these scatter plots be rather well defined. This indirect experimental exploration still requires the identification of elastic supersymmetric events with  $eX + \cancel{p}_T$  signature (in order to identify protons that contribute to the relevant  $z$ -distribution), but does not require a detailed reconstruction of each such event.

One interesting phenomenon in selectron-neutralino production at HERA is the possibility of using polarized electron beams. Since we have seen that  $\sigma(\tilde{e}_R\chi_1^0) \gg \sigma(\tilde{e}_L\chi_{1,2}^0)$ , right-handed beams are expected to be much more active in producing SUSY signals than left-handed beams. To compare the results obtained with R and L polarized beams is a further selection power to disentangle a genuine signal at HERA.



#### 4.2. Sneutrino-chargino production

Unlike selectron-neutralino production, where right-handedly polarized beam electrons yield the largest signal, sneutrino-chargino production can only occur when the electron beam is *not* completely right-handedly polarized, because  $\tilde{\nu}_{eL}$  couples only to left-handed electrons. The allowed decay modes for the channel in Eq. (1.1b) are

$$\tilde{\nu}_e \rightarrow \chi_1^0 \nu_e, \chi_2^0 \nu_e, \chi_1^\mp e_L^\pm, \quad (4.5a)$$

$$\chi_1^- \rightarrow \chi_1^0 l^- \bar{\nu}_l, \chi_1^0 q \bar{q}'. \quad (4.5b)$$

Since the masses of  $\chi_2^0$  or  $\chi_1^-$  are usually larger than the sneutrino mass,  $\tilde{\nu}_e$  can rarely decay to  $\chi_2^0$  or  $\chi_1^-$  and thus decays mostly invisibly. To contribute to the desired  $eX + \cancel{p}_T$  signal, the chargino must decay leptonically. In this model this branching ratio is quite sizeable (see Fig. 2 in Ref. [3]). Moreover, for most points in the allowed parameter space of the model, the daughter electron from the decay of the chargino is hard ( $E_l > 5 \text{ GeV}$ ). For a detail discussion of this point, we refer the reader to Ref. [3]. The cross section for this process, including branching ratios, is shown in Fig. 6 (top (bottom) row for elastic (deep-inelastic) contribution), and can be seen to be of the same order as that for selectron-neutralino production (*c.f.* Figs. 2,3).

The signature for this production channel is different from the selectron-neutralino channel in the following ways: (i) it only produces left-handed daughter leptons (compared to dominantly right-handed ones); and (ii) the daughter leptons can equally likely be of any flavor (as opposed to only electrons). Since  $\chi_1^-$  can also decay likely into hadronically noisy jets, in general, sneutrino-chargino detection is more complicated than selectron-neutralino detection. But “noise” and “complications” could be disentangled since a right-handedly polarized electron beam would shut off this channel completely.

## 5. Discussion and conclusion

We have investigated the relevant SUSY production channels at HERA within the no-scale flipped  $SU(5)$  supergravity model, where direct squark production is highly suppressed. Because of the different masses of  $\tilde{e}_L$  and  $\tilde{e}_R$ , the production rate is dramatically different when the incident electron beam is polarized left-handedly or right-handedly. If it is right-handedly polarized, then the  $\tilde{e}_R \chi_{1,2}^0$  channels will be the only ones allowed, with a hard electron with large  $p_T$  as the dominant signal. If the beam is left-handedly polarized,

only the much smaller  $\tilde{e}_L\chi_{1,2}^0$  channels will contribute, as well as the hadronically noisy  $\tilde{\nu}_e\chi_1^-$  channel. This tuning of the machine would be relevant only after positive sparticle identification. Before that the unpolarized beam will allow for a larger total supersymmetric signal. In Fig. 7 (top row) we show the total elastic plus deep-inelastic  $\tilde{e}_{R,L}\chi_{1,2}^0$  signal versus  $m_{\tilde{e}_R}$ , which would be relevant for right-handed beam polarization. In the bottom row of the same figure we show the *total* supersymmetric cross section into  $eX + \cancel{p}$ , including  $\tilde{e}_{R,L}\chi_{1,2}^0$  and  $\tilde{\nu}_e\chi_1^-$ , versus  $m_{\tilde{e}_R}$ . This plot, and its analogs in Fig. 8 where  $m_{\tilde{e}_R}$  is replaced by  $m_{\chi_1^0}$  and  $m_{\tilde{\nu}_e}$ , show the discovery potential at HERA for a given sensitivity.

Assuming optimal experimental efficiencies and a suppressed or subtracted-off background, with an integrated luminosity of  $\mathcal{L} = 100 (1000) \text{ pb}^{-1}$ , and demanding at least five fully identified events (*i.e.*,  $\sigma > 5 \times 10^{-2} (5 \times 10^{-3}) \text{ pb}$ ), one could probe as high as  $m_{\tilde{e}_R} \approx 70 (90) \text{ GeV}$ ,  $m_{\chi_1^0} \approx 40 (65) \text{ GeV}$ , and  $m_{\tilde{\nu}_e} \approx 70 (125) \text{ GeV}$ . The analogous plots versus  $m_{\chi_1^\pm}$  are not very informative in pinning down the discovery limit in this variable, since it ranges widely  $m_{\chi_1^\pm} \lesssim 50 - 115 (120 - 170) \text{ GeV}$  for  $\mathcal{L} = 100 (1000) \text{ pb}^{-1}$ . The short term discovery limits ( $\mathcal{L} = 100 \text{ pb}^{-1}$ ) would extend the present LEPI lower bounds on these sparticle masses by  $\approx 25 \text{ GeV}$ . The long term discovery limits are competitive with those foreseeable at LEP II [4]. We have also shown that the Leading Proton Spectrometer (LPS) at HERA is an excellent supersymmetry detector which can provide indirect information about the sparticle masses by measuring the leading proton longitudinal momentum distribution in elastic  $e\cancel{p} + p$  processes, without the need to reconstruct all such events. We conclude that HERA is an interesting supersymmetric probe in the no-scale flipped  $SU(5)$  supergravity model.

*Acknowledgments:* This work has been supported in part by DOE grant DE-FG05-91-ER-40633. The work of J.L. has been supported by an SSC Fellowship. The work of D.V.N. has been supported in part by a grant from Conoco Inc. The work of X. W. has been supported by a T-1 World-Laboratory Scholarship. We would like to thank the HARC Supercomputer Center for the use of their NEC SX-3 supercomputer and the Texas A&M Supercomputer Center for the use of their CRAY-YMP supercomputer.

## References

- [1] R. Arnowitt and P. Nath, Phys. Rev. Lett. **69** (1992) 725; P. Nath and R. Arnowitt, Phys. Lett. B **287** (1992) 89 and Phys. Lett. B **289** (1992) 368; J. L. Lopez, D. V. Nanopoulos, and A. Zichichi, Phys. Lett. B **291** (1992) 255; J. L. Lopez, D. V. Nanopoulos, and H. Pois, Phys. Rev. D **47** (1993) 2468; J. L. Lopez, D. V. Nanopoulos, H. Pois, and A. Zichichi, Phys. Lett. B **299** (1993) 262.
- [2] J. L. Lopez, D. V. Nanopoulos, and A. Zichichi, Texas A & M University preprint CTP-TAMU-68/92, CERN-TH.6667/92, and CERN-PPE/92-188.
- [3] J. L. Lopez, D. V. Nanopoulos, X. Wang, and A. Zichichi, Texas A & M University preprint CTP-TAMU-76/92, CERN/LAA/92-023, and CERN-PPE/92-194.
- [4] J. L. Lopez, D. V. Nanopoulos, H. Pois, X. Wang, and A. Zichichi, Texas A & M University preprint CTP-TAMU-89/92, CERN/LAA/93-01, CERN-TH.6773/93, and CERN-PPE/93-16.
- [5] Physics at HERA: proceedings of the Workshop on Physics at HERA, Hamburg, Germany, Oct. 29-30, 1991. Edited by W. Buchmuller, G. Ingelman (DESY, Hamburg, Germany, 1992).
- [6] G. Altarelli, G. Martinelli, B. Mele, and R. Rückl, Nucl. Phys. B **262** (1985) 204.
- [7] M. Drees, and D. Zeppenfeld, Phys. Rev. D **39** (1989) 2536.
- [8] H. Tsutsui, K. Nishikawa, and S. Yamada, Phys. Lett. B **245** (1990) 663.
- [9] C. F. Weizsäcker, Z. Phys. **88**, (1934)612; E. J. Williams, Phys. Rev. **45**, (1934)729.
- [10] For a review see, A. B. Lahanas and D. V. Nanopoulos, Phys. Rep. **145** (1987) 1.
- [11] S. Kelley, J. L. Lopez, D. V. Nanopoulos, H. Pois, and K. Yuan, Texas A & M University preprint CTP-TAMU-16/92 and CERN-TH.6498/92 (to appear in Nucl. Phys. B).
- [12] J. F. Gunion, and H. E. Haber, Nucl. Phys. B **272** (1986) 1.
- [13] J. G. Morfin, and W. K. Tung, Z. Phys. C **52** (1991) 13.

## Figure Captions

- Fig. 1. The Feynman diagrams contributing to the production channels  $e^-p \rightarrow \tilde{e}_{L,R}^- \chi_{1,2}^0 + p$  and,  $e^-p \rightarrow \tilde{\nu}_e \chi_1^- + p$ , through the elastic processes. The relevant deep-inelastic diagrams can be obtained by simply replacing *proton* by *parton*.
- Fig. 2. The elastic cross section for  $e^-p \rightarrow \tilde{e}_R^- \chi_1^0 \rightarrow ep + \not{p}$  versus  $m_{\tilde{e}_R}$  (top row) and  $e^-p \rightarrow \tilde{e}_{R,L}^- \chi_{2,1}^0 \rightarrow ep + \not{p}$  (bottom row). Note the dominance of the former. The corresponding cross section for  $\tilde{e}_L \chi_2^0$  is negligible.
- Fig. 3. The deep-inelastic (DI) cross section for  $e^-p \rightarrow \tilde{e}_R^- \chi_1^0 \rightarrow eX + \not{p}$  versus  $m_{\tilde{e}_R}$  (top row) and  $e^-p \rightarrow \tilde{e}_{R,L}^- \chi_{2,1}^0 \rightarrow ep + \not{p}$  (bottom row). Note the dominance of the former. The corresponding cross section for  $\tilde{e}_L \chi_2^0$  is negligible.
- Fig. 4. The most likely value of the transverse momentum of the daughter electron (weighed by the various elastic cross sections) versus the total elastic cross section for selectron-neutralino production. The daughter electron will be hard and with large  $p_T$ .
- Fig. 5. The most likely value of the relative proton energy loss in elastic processes (weighed by the various elastic cross sections) versus the total elastic cross section for selectron-neutralino production (top row) and  $m_{\tilde{e}_R}$  (bottom row). The Leading Proton Spectrometer (LPS) will allow determination of  $\tilde{z}_{min}$ , and thus an indirect measurement of  $m_{\tilde{e}_R}$ .
- Fig. 6. The elastic and deep-inelastic (DI) cross sections for  $ep \rightarrow \tilde{\nu}_e \chi_1^- \rightarrow ep(X) + \not{p}$  versus  $m_{\chi_1^\pm}$ . Note the faster drop off of the deep-inelastic cross section. This same phenomenon occurs for selectron-neutralino production.
- Fig. 7. The elastic plus deep-inelastic selectron-neutralino cross section versus  $m_{\tilde{e}_R}$  (top row). This signal will be the dominant one for a right-handedly polarized electron beam. Also (bottom row) the elastic plus deep-inelastic total supersymmetric cross section (including selectron-neutralino and sneutrino-chargino channels) versus  $m_{\tilde{e}_R}$ , showing the discovery potential at HERA on this mass variable.
- Fig. 8. The discovery potential at HERA (*i.e.*, the total supersymmetric cross section) for the lightest neutralino (top row) and the sneutrino (bottom row).

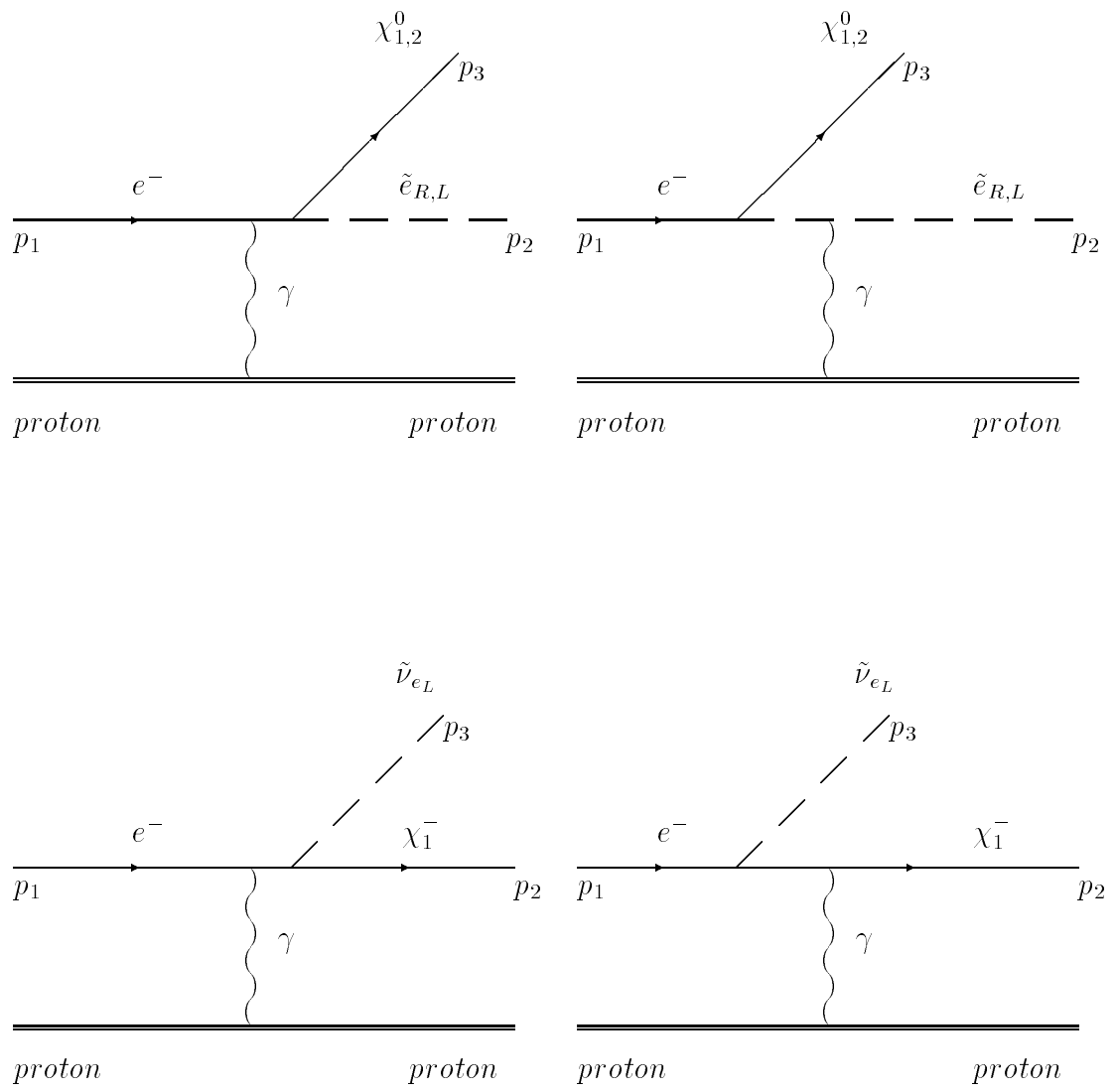


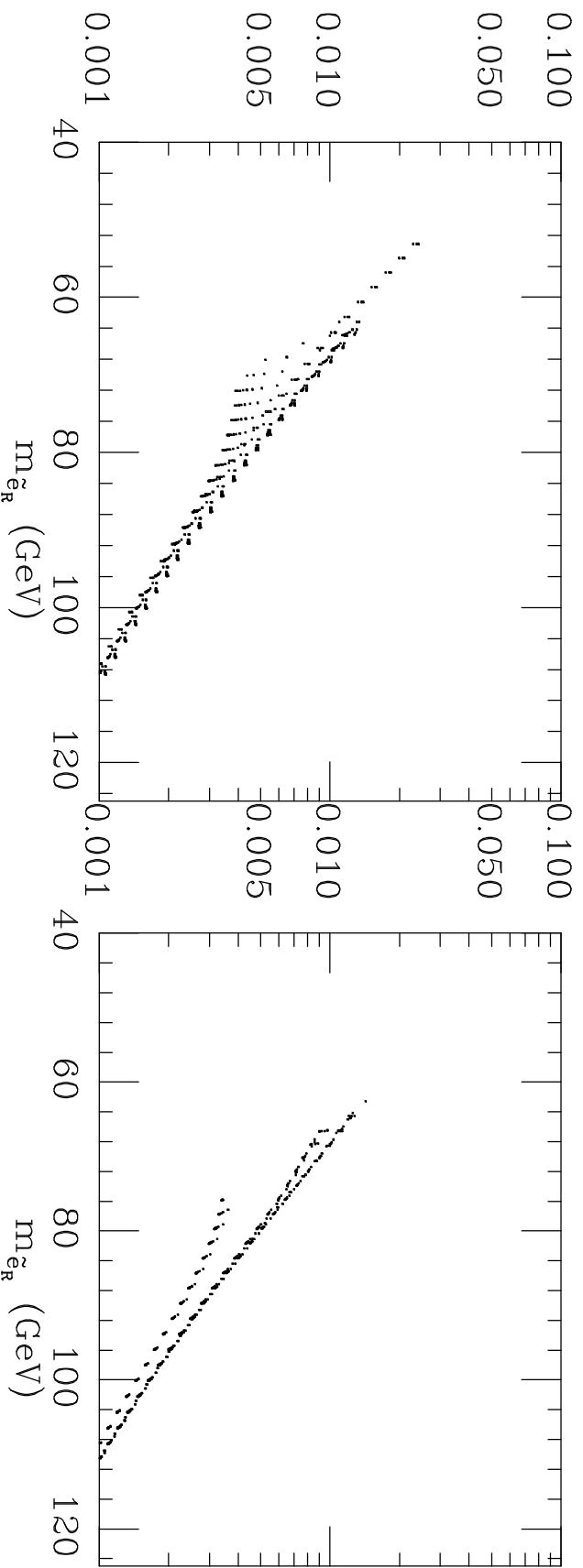
Figure 1

$\mu > 0$ 

flipped SU(5)

 $\mu < 0$ 

$$\sigma_{\text{el}}(ep \rightarrow \tilde{e}_R \chi_1^0 \rightarrow ep + \cancel{p}) \text{ pb}$$



$$\sigma_{\text{el}}(ep \rightarrow \tilde{e}_{R,L} \chi_{2,1}^0 \rightarrow ep + \cancel{p}) \text{ pb}$$

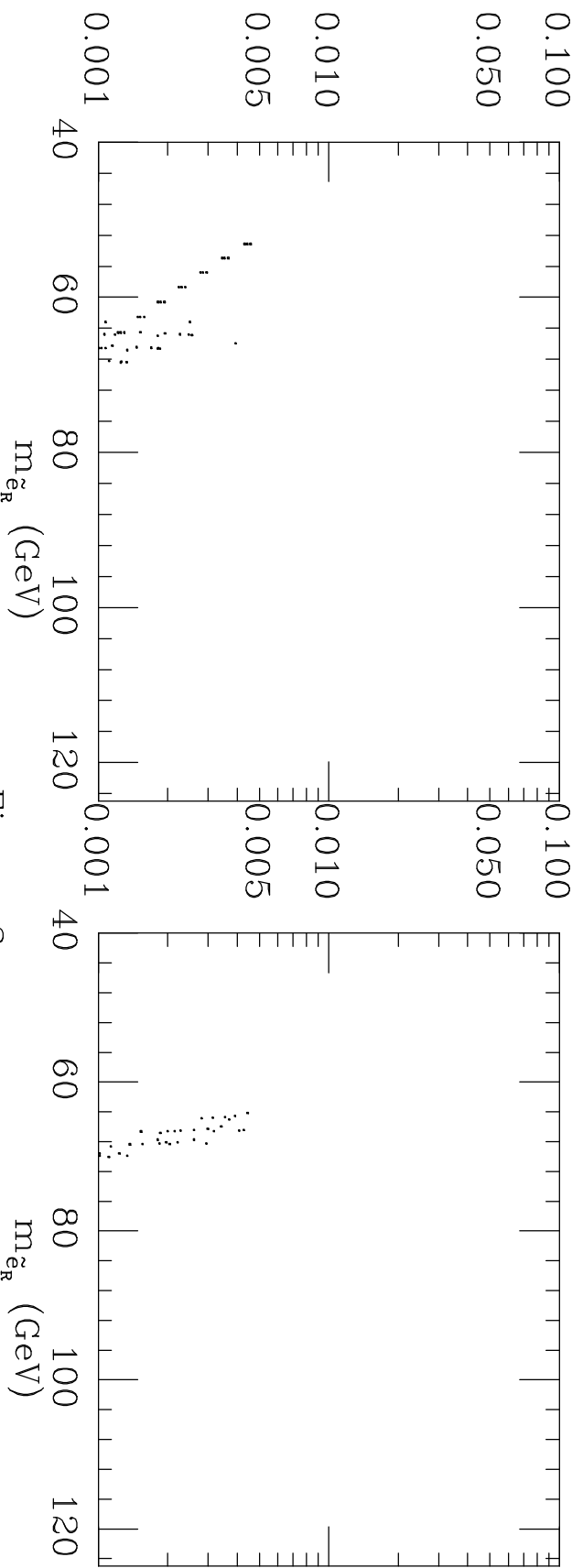


Figure 2

$\mu > 0$ 

flipped SU(5)

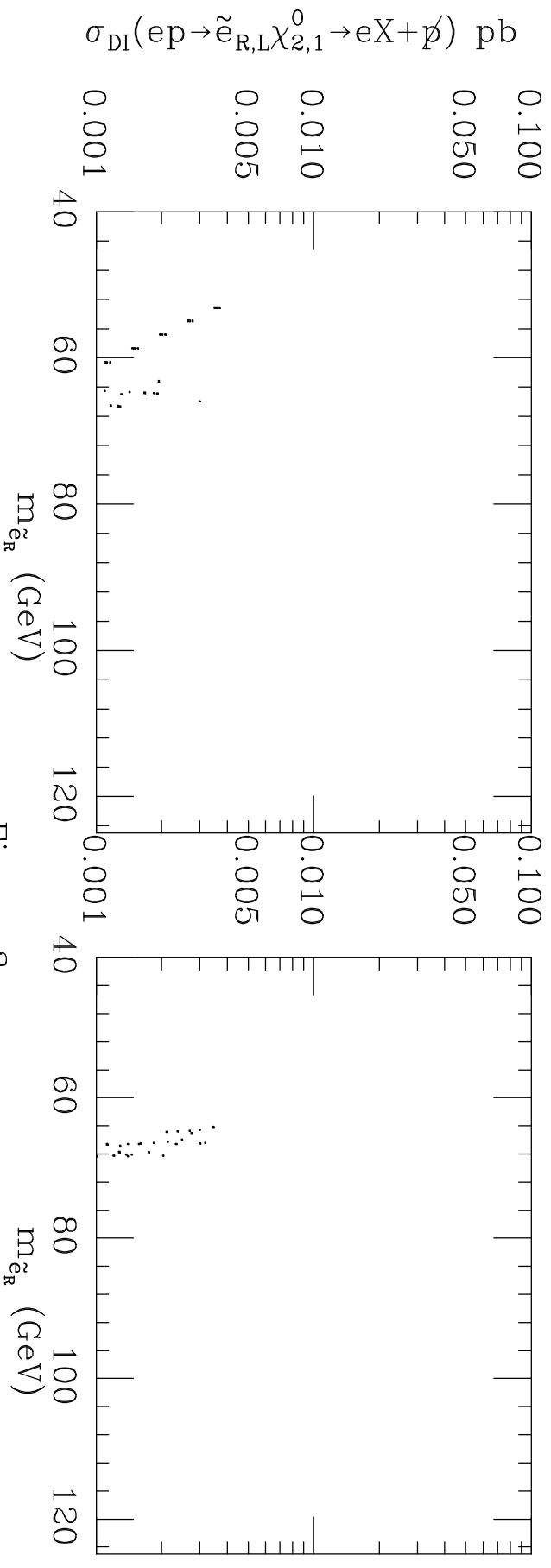
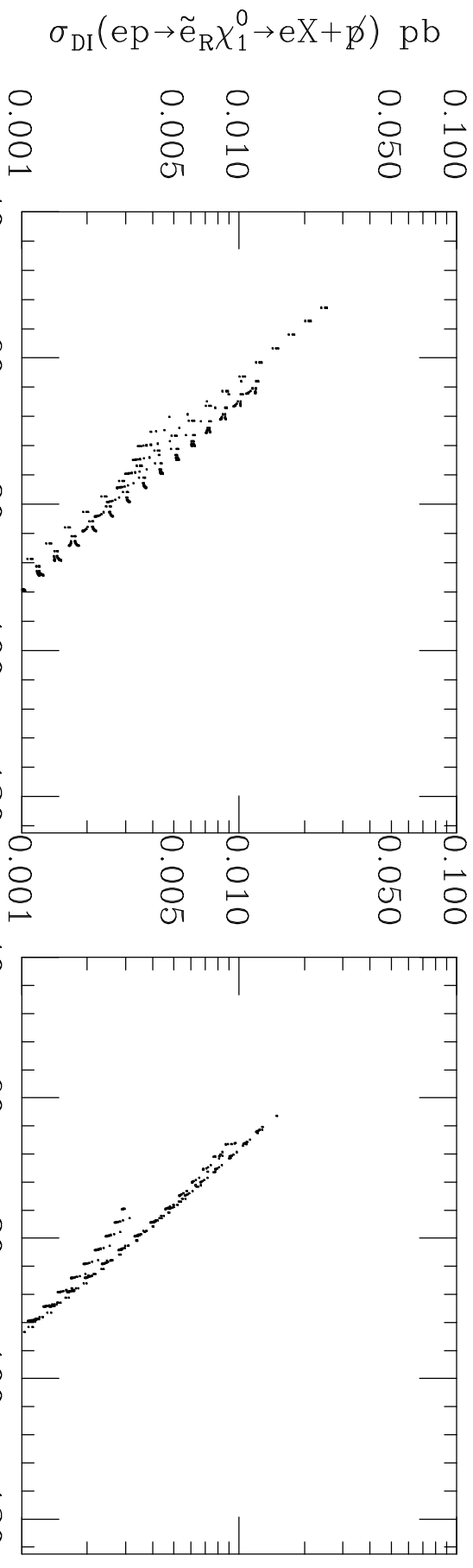
 $\mu < 0$ 

Figure 3

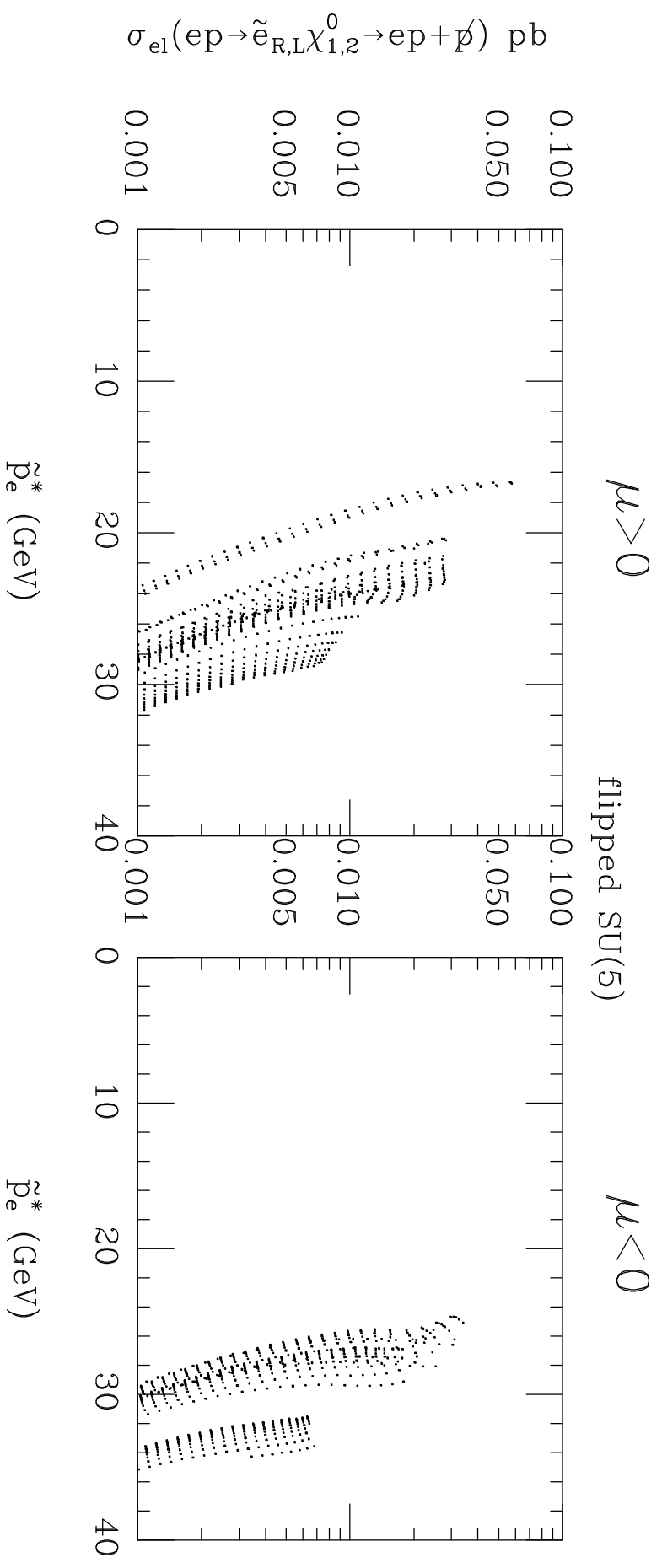


Figure 4



$\mu > 0$ 

flipped SU(5)

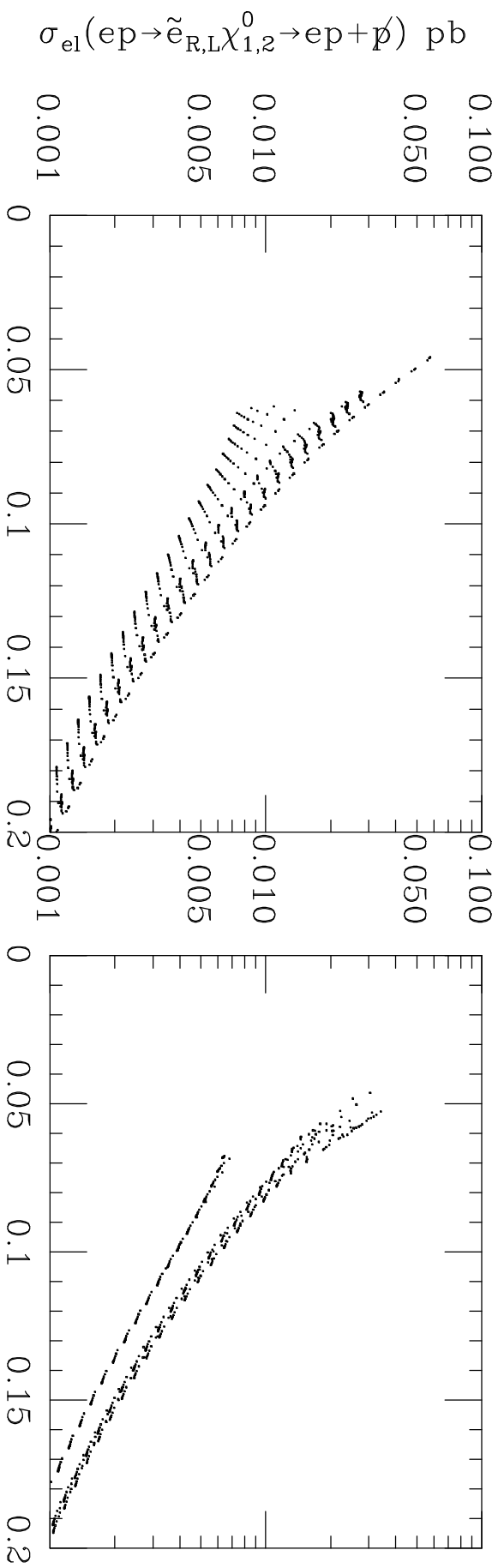
 $\mu < 0$ 

Figure 5

$\mu > 0$ 

flipped SU(5)

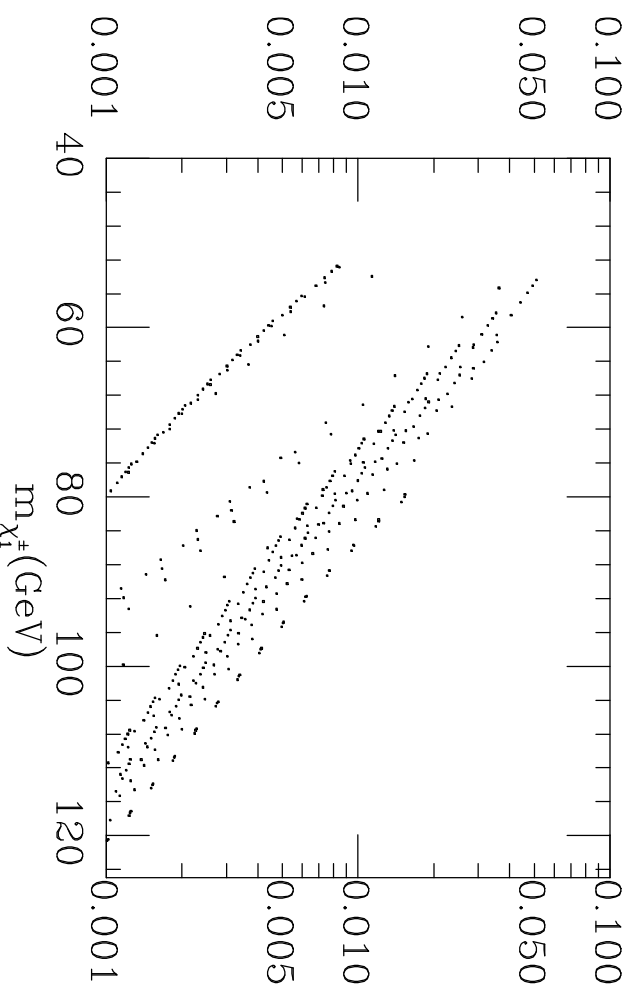
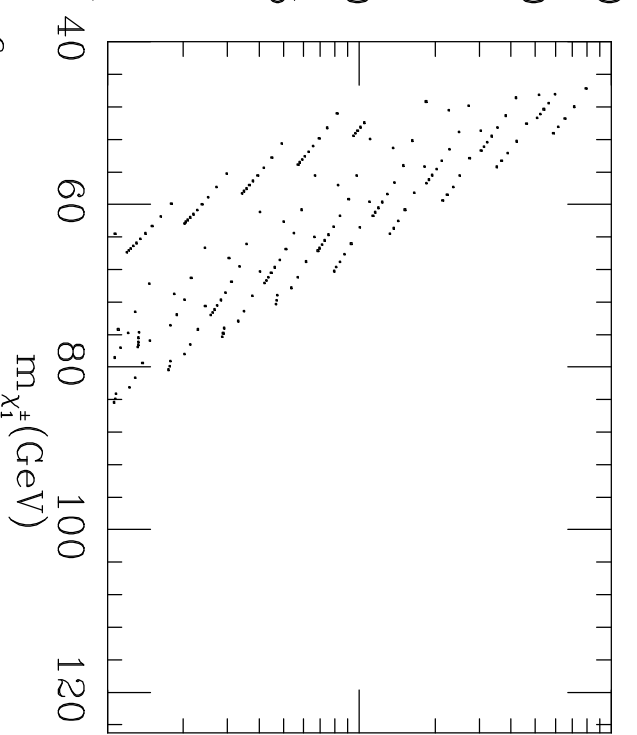
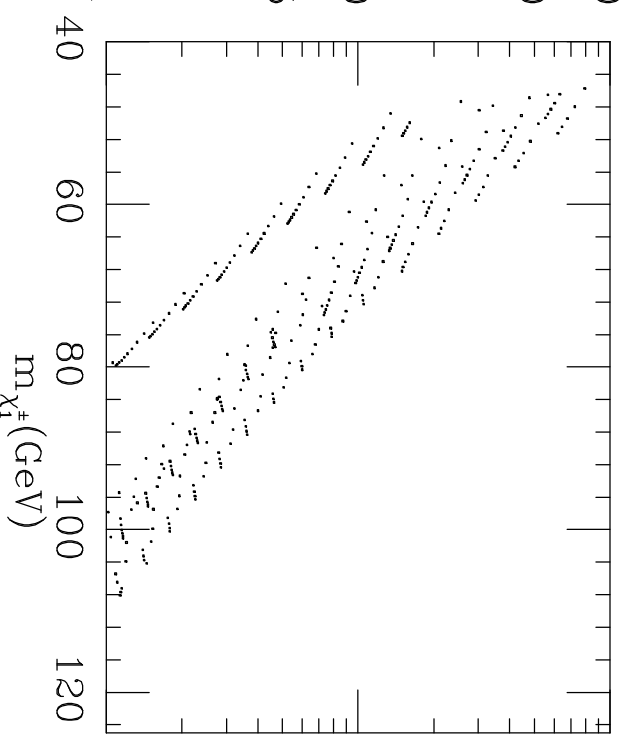
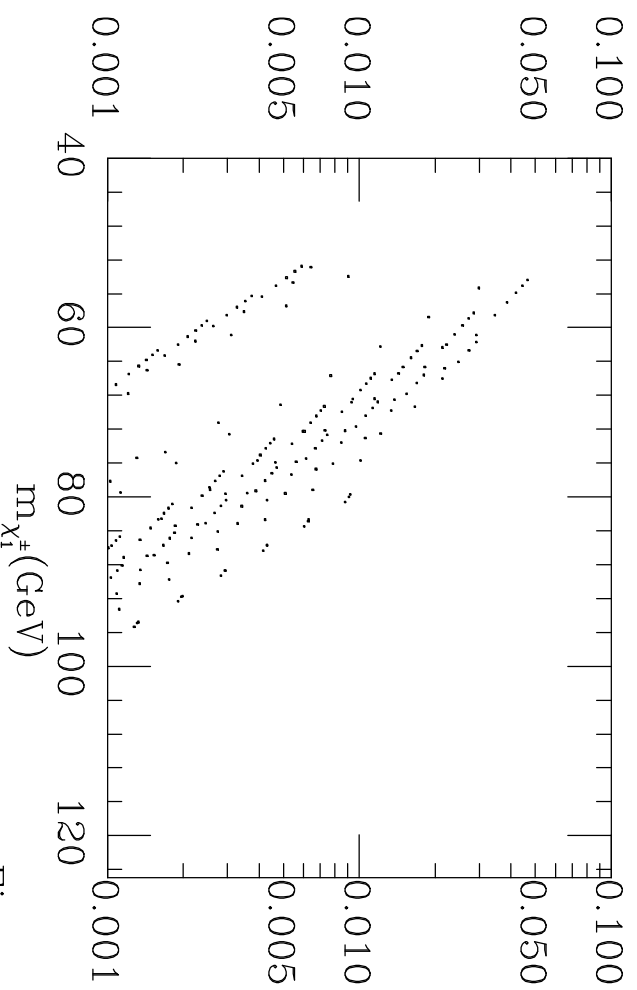
 $\mu < 0$  $\sigma_{\text{el}}(ep \rightarrow \tilde{\nu}_e \chi_1^- \rightarrow ep + \cancel{p'})$  pb $\sigma_{\text{DI}}(ep \rightarrow \tilde{\nu}_e \chi_1^- \rightarrow eX + \cancel{p'})$  pb

Figure 6

$\mu > 0$ 

flipped SU(5)

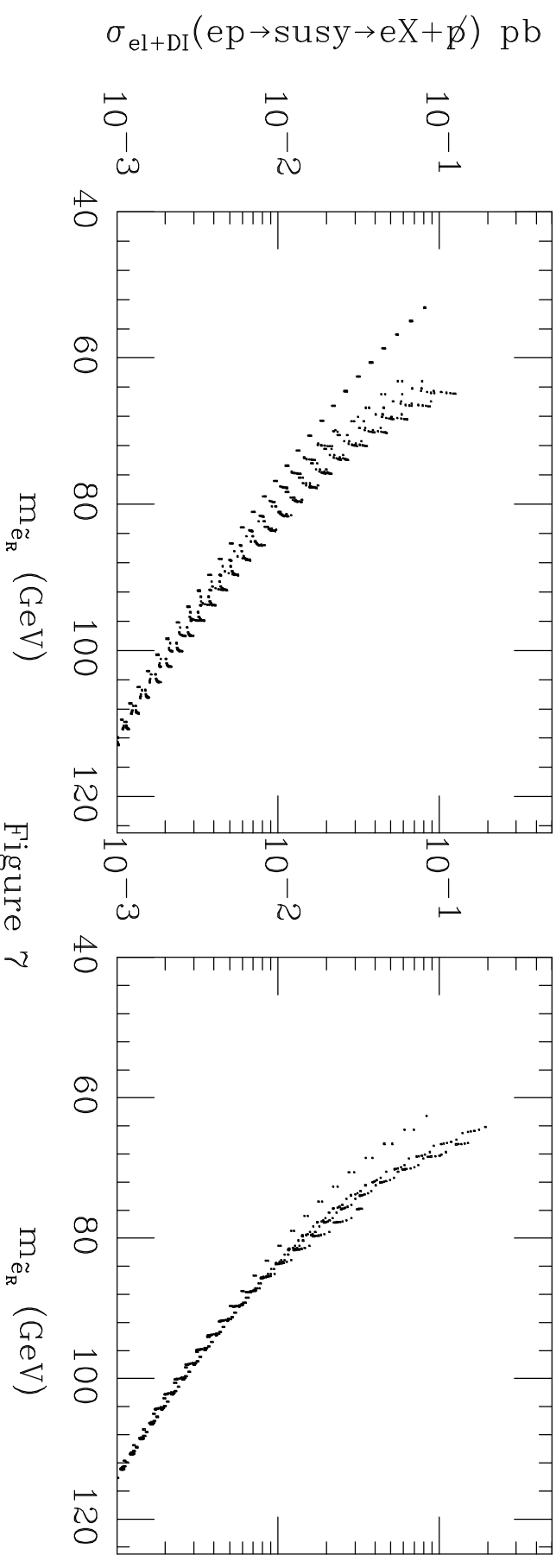
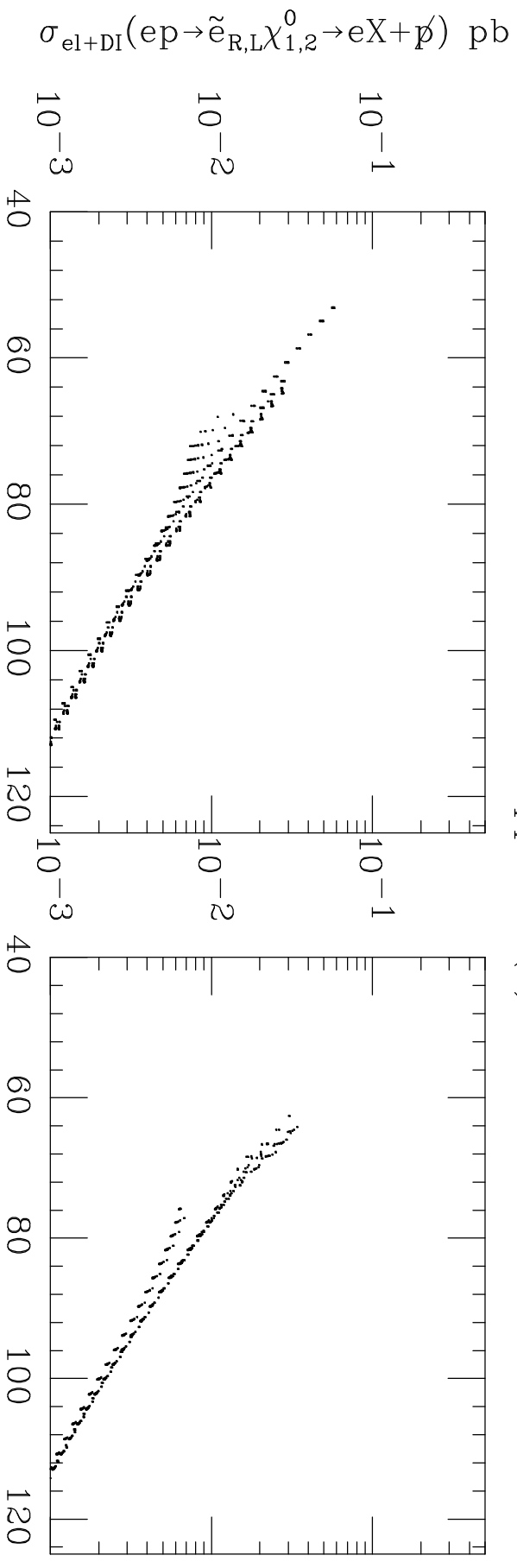
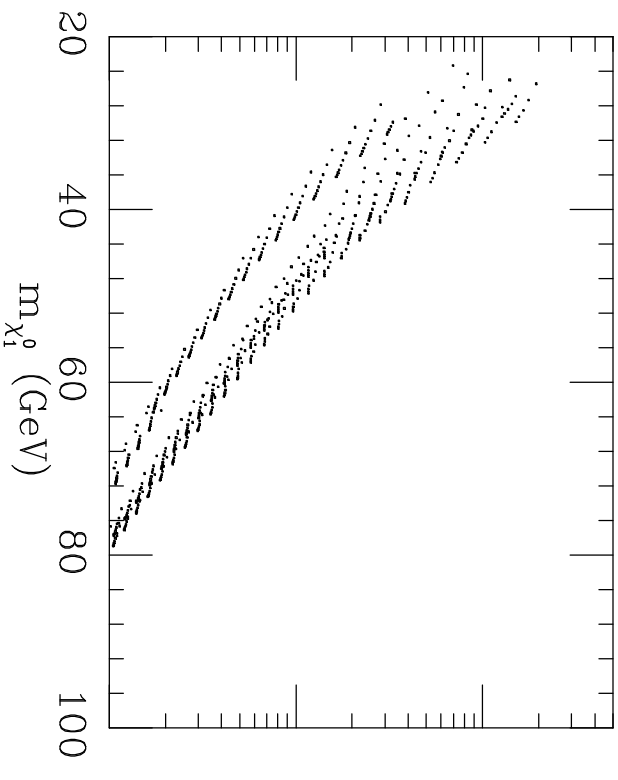
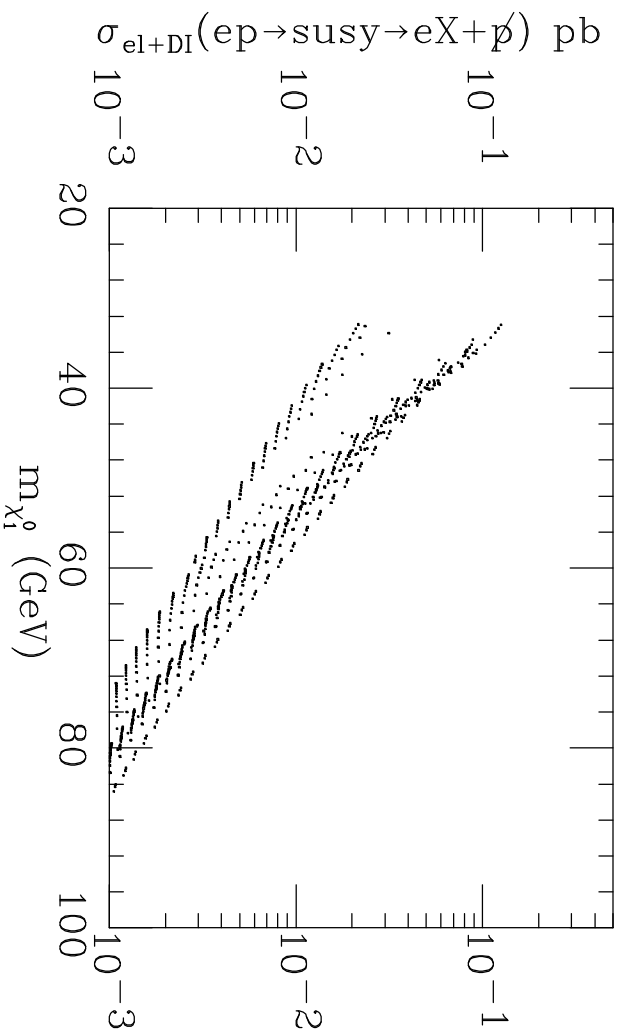
 $\mu < 0$ 

Figure 7

$\mu > 0$   
flipped SU(5)



$\mu < 0$

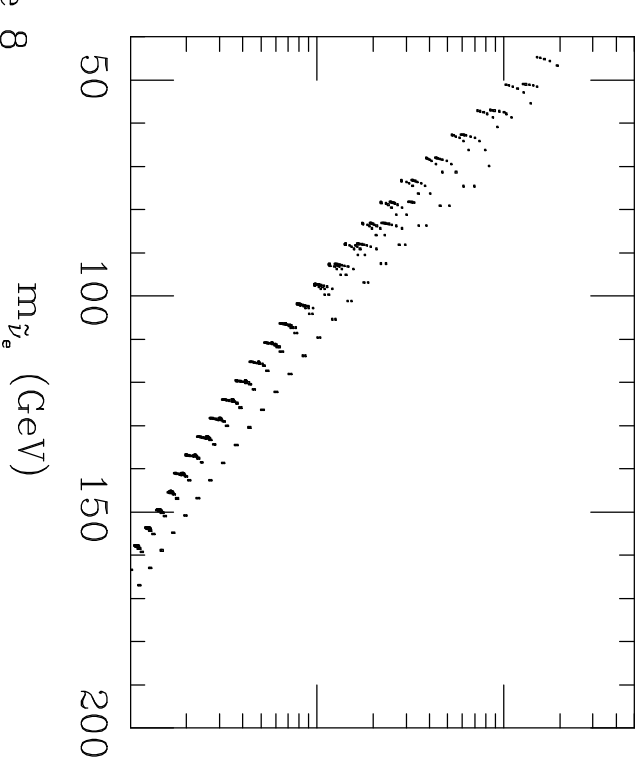
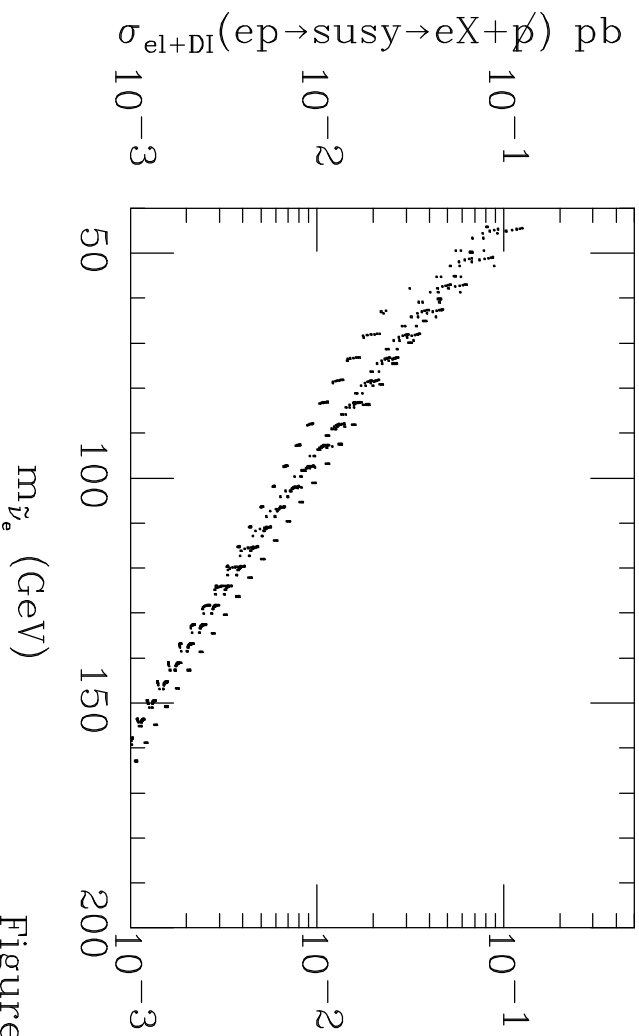


Figure 8